



Electrochemical and spectroscopic properties of twisted dibenzo[*g,p*]chrysene derivatives

Tomoya Imai¹, Ryuhei Akasaka², Naruhiro Yoshida², Toru Amaya^{*1} and Tetsuo Iwasawa^{*2}

Full Research Paper

Open Access

Address:

¹Department of Information and Basic Science, Graduate School of Science, Nagoya City University, 1, Yamanohata, Mizuho-cho, Mizuho-ku, Nagoya, Aichi 467-8501, Japan and ²Department of Materials Chemistry, Ryukoku University, Seta, Otsu, Shiga, 520-2194, Japan

Email:

Toru Amaya^{*} - amaya@nsc.nagoya-cu.ac.jp; Tetsuo Iwasawa^{*} - iwasawa@rins.ryukoku.ac.jp

* Corresponding author

Keywords:

DFT calculation; dibenzo[*g,p*]chrysenes; fluorescent compounds; oxidation; polycyclic aromatic hydrocarbon (PAH); twisted acenes

Beilstein J. Org. Chem. **2022**, *18*, 963–971.

<https://doi.org/10.3762/bjoc.18.96>

Received: 04 June 2022

Accepted: 20 July 2022

Published: 03 August 2022

This article is part of the thematic issue "Molecular and macromolecular electrochemistry: synthesis, mechanism, and redox properties".

Guest Editor: S. Inagi

© 2022 Imai et al.; licensee Beilstein-Institut.

License and terms: see end of document.

Abstract

Dibenzo[*g,p*]chrysene (DBC), which consists of a twisted naphthalene core with four fused benzene rings, is a promising framework for organic electronic materials. Therefore, the research for structure–property relationships is important for the design of DBC-based materials. Here, the electrochemical and spectroscopic properties of DBC derivatives were investigated, and the effects of substituents and torsion of the naphthalene moiety were examined based on density functional theory (DFT) calculations. All the substituted DBC derivatives showed higher oxidation potentials than that for **DBC-H**, even for compounds that contained an electron-donating group such as **DBC-Me** and **DBC-SMe**. DFT calculations clearly indicate that these higher oxidation potentials are due to the ineffective conjugation of the MeO group, which is oriented perpendicular to the benzene ring because of the steric repulsion of substituents on both sides. More specifically, the inductive effect of the MeO group is dominant rather than the mesomeric effect when the substituent is located at both sides of the MeO group. Concerning the torsion of the naphthalene moiety, the twisting results in a slight increase in the HOMO and a slight lowering of the LUMO. The twisting effect is much smaller than the conjugation effect of the MeO group. Absorption spectra of all the substituted DBC derivatives also showed a red-shift as compared to that for **DBC-H**. Concerning the luminescence, a strong photoluminescence was observed for **DBC-H** and **DBC-Si**.

Introduction

Polycyclic aromatic hydrocarbons (PAHs) have attracted interest as potential electronic and optoelectronic materials [1–12]. Non-planar PAHs have been extensively investigated

from the viewpoint of their synthetic challenge and/or for the development of functional organic materials [13–22]. Among such PAHs, twisted acenes are an interesting class

of compounds due to their characteristic structures and conjugation systems [23–25]. Dibenzo[*g,p*]chrysene (DBC), which consists of a twisted naphthalene core with four fused benzene rings (Figure 1a) [26], is a promising framework for serving as organic semiconductors, dyes, liquid crystals, and light-emitting materials. A number of substituted DBCs have been reported in this context [27–46]. To develop charge-transport materials, Rathore et al. reported on the stability of radical cations of DBCs with MeO groups located at X and/or Y (**MeO-DBC-1**, **MeO-DBC-2**, and **MeO-DBC-3**, Figure 1b) [43]. The first oxidation potential

(E_{ox1}) of **MeO-DBC-1** was reported to be 0.40 V (based on Fc/Fc⁺), which is 0.48 V lower than that of **DBC**. In contrast, when a MeO group is introduced at the X position (**MeO-DBC-2**), the E_{ox1} is lower by only 0.15 V than that of **DBC**. It has also been reported that the oxidation potential of **MeO-DBC-3**, in which the MeO groups are attached at both X and Y, is 0.06 V higher than that for **MeO-DBC-1**. These remarkable substituent effects are an interesting and important finding for molecular design, but the effects of X and Z substituents and the twisting of the naphthalene moiety have not been reported.

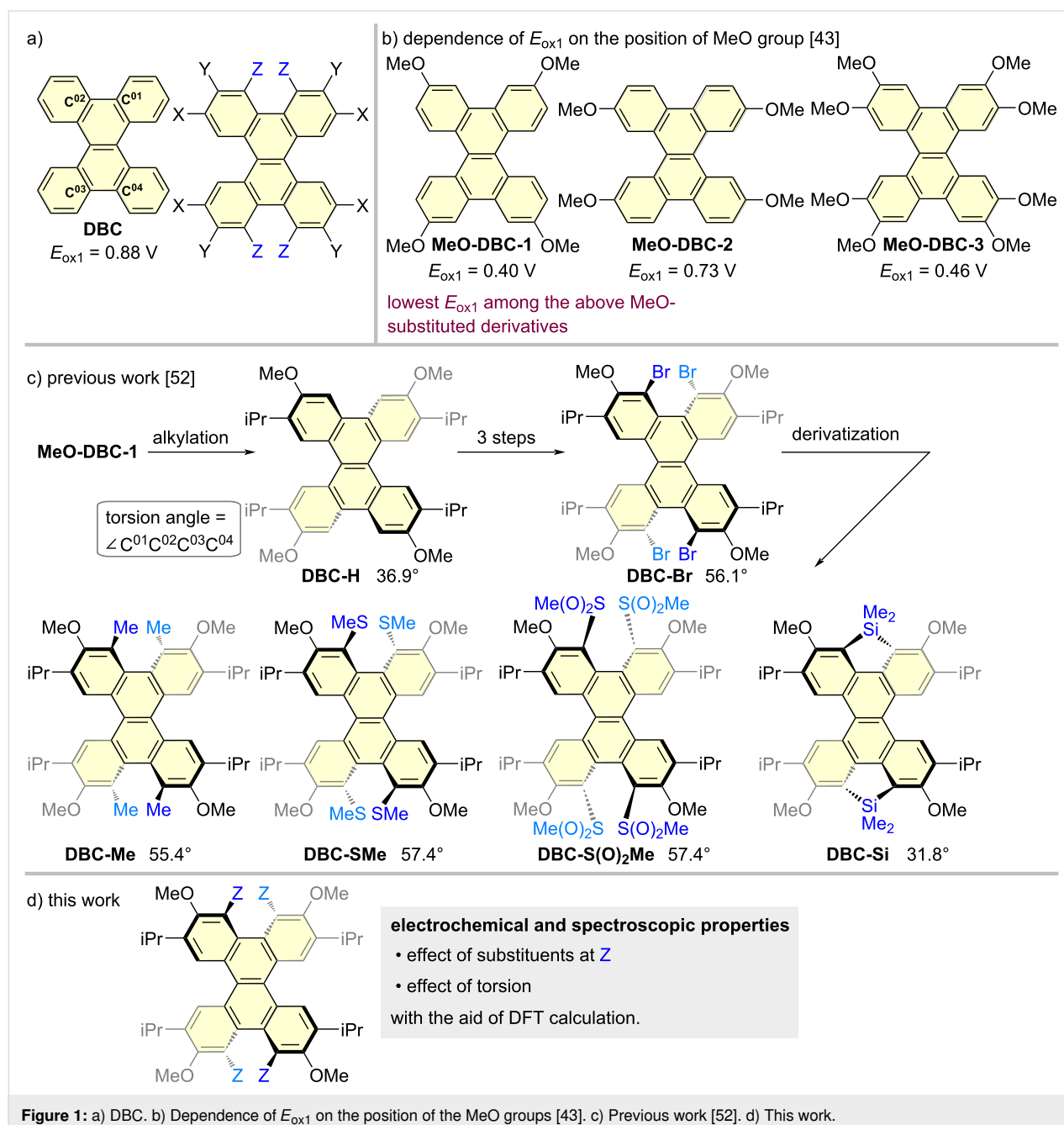


Figure 1: a) DBC. b) Dependence of E_{ox1} on the position of the MeO groups [43]. c) Previous work [52]. d) This work.

We previously studied the synthesis of solution-processable DBC derivatives with various substituents attached [47–51]. We also recently reported on a synthetic strategy for preparing DBC derivatives using **DBC-H** with four isopropyl groups at X as a key template for the derivatization (Figure 1c). Based on this strategy, various substituents were introduced at Z to produce **DBC-Br**, **DBC-Me**, **DBC-SMe**, **DBC-S(O)₂Me**, and **DBC-Si** (Figure 1c) [52]. The structures of all these derivatives were determined by X-ray crystallographic analysis, in which torsion angles were varied in a range from 31.8° (**DBC-Si**) to 57.4° (**DBC-S(O)₂Me**) [52]. These DBC derivatives have four methoxy moieties at the Y position, which aroused our interest concerning the stability of those oxidation states.

Herein, we report on the electrochemical and spectroscopic properties of the DBC derivatives, where the effects of substitu-

ents and torsion were examined with the aid of DFT calculations. Consequently, the findings revealed that the substitution at the Z position induces a change in the conformation of the MeO groups, making the conjugation of the MeO groups ineffective, thus resulting in the lowering of both HOMO and LUMO energy levels. Concerning the twisting, the effect to the HOMO and LUMO energy levels was found to be small. We anticipate that the impact of diverse substituents and torsion angles on the chemical properties would be beneficial in terms of creating DBC-based materials.

Results and Discussion

Electrochemical properties

Cyclic voltammograms (CVs) and square-wave voltammograms (SWVs) were measured for **DBC-H**, **DBC-Me**, **DBC-SMe**, **DBC-Br**, **DBC-S(O)₂Me**, and **DBC-Si** (Figure 2)

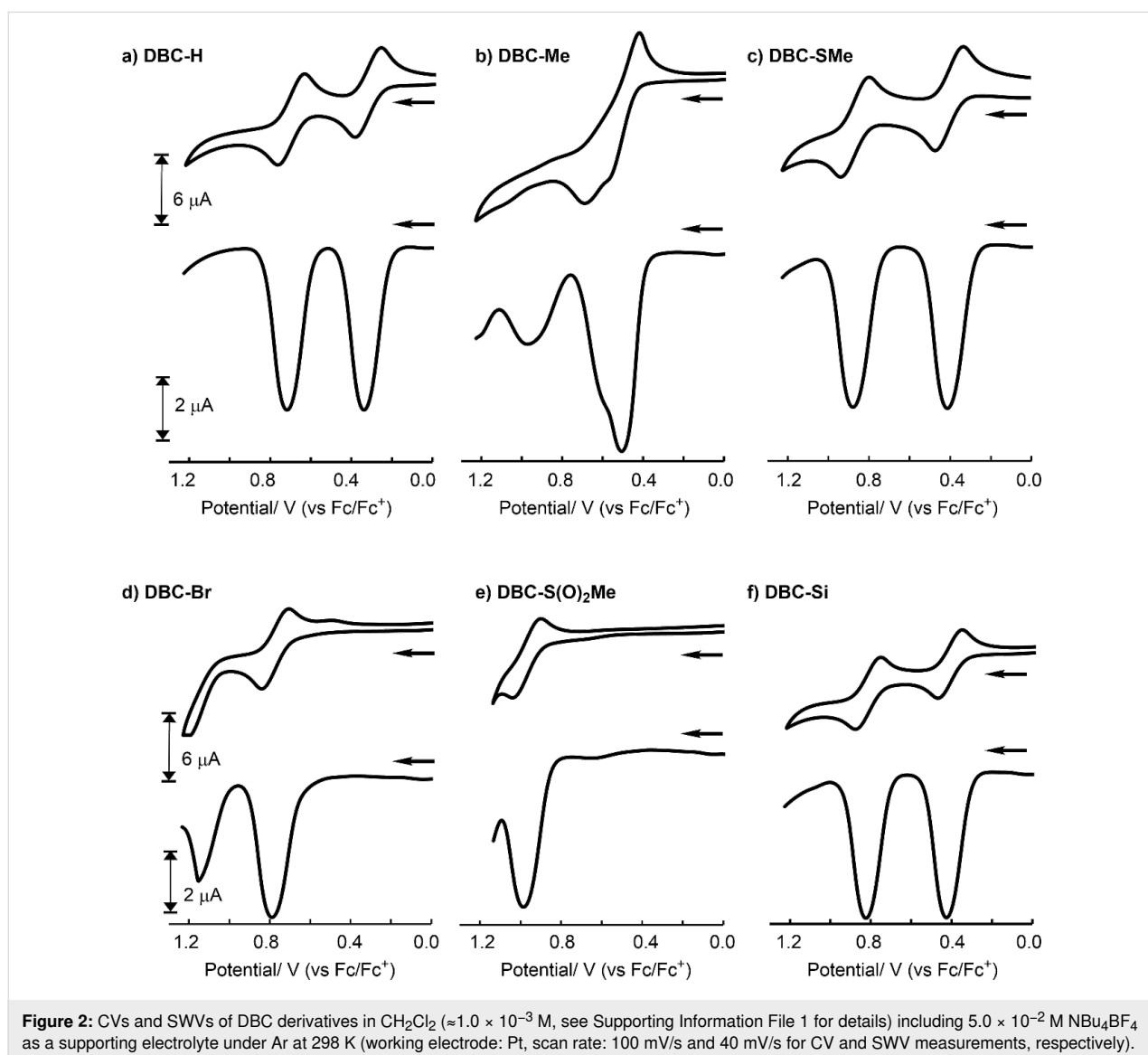


Figure 2: CVs and SWVs of DBC derivatives in CH_2Cl_2 ($\approx 1.0 \times 10^{-3}$ M, see Supporting Information File 1 for details) including 5.0×10^{-2} M NBu_4BF_4 as a supporting electrolyte under Ar at 298 K (working electrode: Pt, scan rate: 100 mV/s and 40 mV/s for CV and SWV measurements, respectively).

[53]. Table 1 summarizes the first and second oxidation potentials based on Fc/Fc^+ ($E_{\text{ox}1}$ and $E_{\text{ox}2}$) determined from the SWVs, together with the torsion angles determined from the X-ray crystal structures [52], the HOMO and LUMO levels determined from DFT calculations [52,54] and estimated based on $E_{\text{ox}1}$. The voltammogram of **DBC-H** exhibited a reversible, two-step, two-electron redox process, with $E_{\text{ox}1}$ and $E_{\text{ox}2}$ values of 0.34 V and 0.72 V, respectively (Figure 2a). The value of $E_{\text{ox}1}$ is 0.06 V lower than that of **MeO-DBC-1** which does not contain isopropyl groups. This is in contrast to **MeO-DBC-3**, in which four MeO groups are introduced in place of the isopropyl groups, which has a 0.06 V higher oxidation potential than that of **MeO-DBC-1**. This indicates that alkyl substituents in the X position are effective in stabilizing the radical cation, thus making it more susceptible to oxidation. Unlike **DBC-H**, an irreversible voltammogram was observed in case of **DBC-Me** (Figure 2b). The first oxidation potential obtained from the SWV was 0.51 V, which is 0.17 V higher than that of **DBC-H**. This higher oxidation potential is somewhat surprising, which is discussed in the next paragraph based on DFT calculations. The CV of **DBC-SMe** showed a reversible two-electron redox process, with $E_{\text{ox}1}$ and $E_{\text{ox}2}$ values of 0.41 V and 0.88 V, respectively (Figure 2c) [53]. It is interesting to note that **DBC-SMe** exhibited a higher oxidation potential than **DBC-H** despite the electron-donating nature due to mesomeric effects based on lone pairs of sulfur atoms. In the CV of **DBC-Br**, a one-electron redox was observed as a reversible process, but a second redox process was not observed (Figure 2d). On the other hand, both the first and second oxidation processes were observed in the SWV of **DBC-Br** ($E_{\text{ox}1}$ and $E_{\text{ox}2}$ are 0.79 V and 1.15 V, respectively). **DBC-S(O)₂Me** with the electron-withdrawing substituents resulted in a reversible oxidation wave, but only a one-electron redox process could be observed due to the limitations of the solvent (Figure 2e). The potential of 0.98 V is the highest among the compounds measured in this study. To investigate the reduction behaviour, **DBC-S(O)₂Me**

was measured in the low potential region. A peak, which appeared to be the one-electron reduction peak, was observed at -2.25 V (see Figure S1 in Supporting Information File 1). Finally, the CV of the silole-fused **DBC-Si** was investigated and the results indicated a reversible two-electron redox process ($E_{\text{ox}1}$ and $E_{\text{ox}2}$ are 0.43 V and 0.82 V, respectively, Figure 2f). These values for $E_{\text{ox}1}$ and $E_{\text{ox}2}$ for **DBC-Si** are slightly higher than those of **DBC-H**. The obtained electrochemical data were nearly consistent with the trend of the values for HOMO obtained based on DFT calculations.

Theoretical calculations

DFT calculations were performed to clarify the reasons for the oxidation potentials [52,54,56]. To investigate the effects of the torsion of the naphthalene moiety and the conformation of the MeO group on the oxidation potential of these materials, hypothetical compounds **DBC-H(56°)-1** and **DBC-H(56°)-2** were created, respectively. In **DBC-H(56°)-1**, the atoms are fixed except for the Me group of **DBC-Me** (torsion angle = 56.5°), and the Me group is changed to H. **DBC-H(56°)-2** is the same structure as **DBC-H(56°)-1** except for the MeO group conformation. Optimizations of **DBC-H(56°)-1** and **DBC-H(56°)-2** based on DFT calculations were performed by fixing the atoms, as described above [56]. The conformations of the MeO group in **DBC-H(56°)-1** and **DBC-H(56°)-2** are nearly perpendicular (98.3°) to and parallel (179.8°) to the benzene ring, respectively (Figure 3 and Table 2). The results were compared to those for **DBC-H** and **DBC-Me** (Figure 3). To examine the torsional effect, **DBC-H** (torsion angle = 39.0°) and **DBC-H(56°)-2** (torsion angle = 56.5°) were compared. The HOMO level of the highly twisted **DBC-H(56°)-2** was 0.09 eV higher than that of the less twisted **DBC-H**. Conversely, the LUMO level of the highly twisted **DBC-H(56°)-2** was 0.05 eV lower than the less twisted **DBC-H**. As a result, the HOMO–LUMO gap of **DBC-H(56°)-2** becomes smaller than that of **DBC-H**. This is consistent with the trend reported for twisted acenes [57]. The

Table 1: Electrochemical data, torsion angles determined from the X-ray crystal structures, and HOMO and LUMO levels for DBC derivatives^a.

compounds	$E_{\text{ox}1}$ [V] ^b	$E_{\text{ox}2}$ [V] ^b	torsion angle [$^\circ$] ^c	HOMO [eV] ^d (the estimated values based on experimental data in parentheses) ^e	LUMO [eV] ^d
DBC-H	0.34	0.72	36.9	-4.64 (-5.4)	-0.87
DBC-Me	0.51	0.96	55.4	-4.81 (-5.6)	-1.22
DBC-SMe	0.41	0.88	57.4	-5.00 (-5.5)	-1.42
DBC-Br	0.79	1.15	56.1	-5.24 (-5.9)	-1.71
DBC-S(O)₂Me	0.98	–	57.4	-5.56 (-6.1)	-2.00
DBC-Si	0.43	0.82	31.8	-4.80 (-5.5)	-1.09

^aConcentration: Around 1.0×10^{-3} M in CH_2Cl_2 (for detailed values, see Supporting Information File 1) containing 5.0×10^{-2} M NBu_4BF_4 as a supporting electrolyte. SWVs were recorded at a platinum electrode at 298 K under Ar. ^bBased on Fc/Fc^+ . ^cThe values obtained from X-ray crystallographic analyses [52]. ^dThe values obtained from DFT calculations at B3LYP6-31G(d,p) [52,54]. ^eThe energy values of HOMO were estimated based on the following equation $E_{\text{HOMO}} = -(E_{\text{ox}1} \text{ vs } \text{Fc}^+/\text{Fc} + 5.1)$ [55].

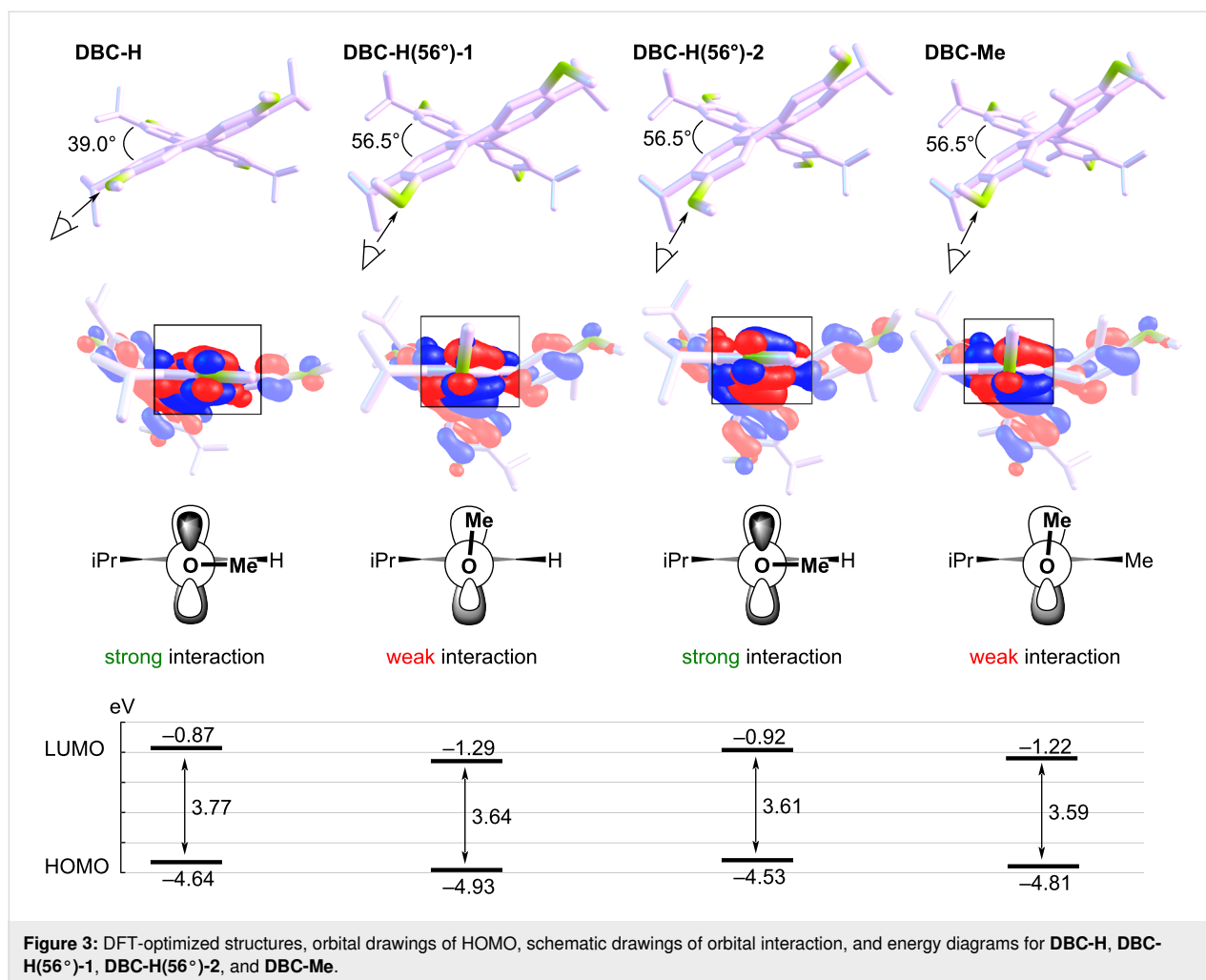
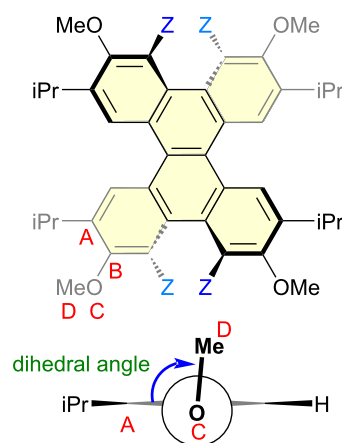


Table 2: Dihedral angles for the DFT-optimized structures of DBC derivatives [B3LYP6-31G(d,p)].

compounds	substituent Z	dihedral angle of ABCD [°]
DBC-H	H	179.6
DBC-H(56°)-1	H	98.3
DBC-H(56°)-2	H	179.8
DBC-Me	Me	98.3
DBC-SMe	SMe	105.7
DBC-Br	Br	111.1
DBC-S(O) ₂ Me	S(O) ₂ Me	97.8
DBC-Si	-SiMe ₂ -	156.6



conformational effect of the MeO group was investigated by comparison of DBC-H(56°)-1 (perpendicular to the benzene ring, 98.3°) with DBC-H(56°)-2 (parallel to the benzene ring,

179.8°). Consequently, both the HOMO and LUMO levels of DBC-H(56°)-2 are higher than those of DBC-H(56°)-1 by -0.40 eV and -0.37 eV, respectively. This is likely attributed by

the effect of conjugation for the orbital of an oxygen atom as shown in the schematic drawing in Figure 3. When the conformation of the MeO group is almost parallel to the benzene ring, the strong orbital interaction between the orbitals on the oxygen and adjacent carbon atoms is possible in HOMO (the orbital drawings are also shown in Figure S2 in Supporting Information File 1). In this case, the mesomeric effect of an oxygen atom is dominant. On the other hand, when the conformation of the MeO group is almost perpendicular to the benzene ring, the interaction between orbitals on the oxygen and adjacent carbon atoms becomes weak in the case of HOMO. In this case, the inductive effect of an oxygen atom can be dominant. Thus, the substituents at the Z position allow the MeO group to be oriented perpendicular to the benzene ring, which results in the lowering of both the HOMO and LUMO (Figure 3). In **DBC-Me**, the lowering of the HOMO based on the inductive effect offsets the increase in HOMO due to the electron-donating nature of the Me group. This can account for the observed higher E_{ox1} for **DBC-Me** than that for **DBC-H**.

Other derivatives were also examined. The dihedral angles are summarized in Table 2. The MeS group is an electron-donating group and may increase the HOMO, but the HOMO level of **DBC-SMe** is lower than that of **DBC-H**, as shown in the electrochemical study and by DFT calculations (Table 1). This is considered to be due to the contribution of the inductive effect of the MeO group by ineffective conjugation. In **DBC-Br** and **DBC-S(O)₂Me**, both the HOMO and LUMO are lower, which can be attributed to the combined effects of their electron-withdrawing by Br and S(O)₂Me groups and ineffective conjugation of the MeO group. In the case of **DBC-Si**, where the dihedral angle of the MeO group is 156.6°, both the HOMO and

LUMO are lower than those for **DBC-H**. Although it is not perpendicular, the lower energy levels for HOMO and LUMO can be accounted for by the ineffective conjugation of the MeO group.

Spectroscopic properties

Absorption and photoluminescence spectra and the simulations of absorption based on TD-DFT calculations [58] are shown in Figure 4 (see Figure S3 in Supporting Information File 1 for excited spectra). The spectral data are summarized in Table 3. The TD-DFT calculations reproduce the absorption spectra quite well. The longest absorption peak is attributed to the transition from HOMO to LUMO and HOMO-1 to LUMO+1 (see Tables S1–S6 in Supporting Information File 1). The trend for the order of optical band gap is roughly consistent with that of the HOMO–LUMO gap obtained from DFT calculation [52].

In the photoluminescence spectra, the luminescence of **DBC-Br** was very weak. On the other hand, **DBC-H**, **DBC-Me**, and **DBC-Si** showed relatively strong photoluminescences with quantum yields of 28%, 21%, and 11%, respectively (Table 3). The photoluminescence wavelengths were shifted toward longer wavelengths in the order of **DBC-Si**, **DBC-H**, **DBC-Me**, **DBC-SMe**, and **DBC-S(O)₂Me**. Of these, the Stokes shift for **DBC-S(O)₂Me** was the largest, which is due to the electron-withdrawing nature of the S(O)₂Me group.

Conclusion

The electrochemical and spectroscopic properties of DBC derivatives were investigated, and the effects of substituents and torsion of the naphthalene moiety were discussed based on DFT calculations. It was also found that introducing a substituent at

Table 3: Absorption and photoluminescence spectral data of DBC derivatives in CH₂Cl₂.

compounds	absorption λ_{max} [nm] molar absorption coefficient ϵ [M ⁻¹ ·cm ⁻¹] in parentheses	optical band gap ^a [eV]	photoluminescence λ_{max} [nm]	quantum yield [%] ^b
DBC-H	363 (16200)	2.95	416	28
DBC-Me	381 (20300)	2.91	427	21
DBC-SMe	384 (16500)	2.88	433	3
DBC-Br	386 (16100)	2.86	– ^c	– ^c
DBC-S(O)₂Me	380 (12900)	2.82	455	6
DBC-Si	368 (9500)	2.97	413	11

^aEstimated from the absorption edge. ^bMeasured based on the absolute quantum yield method using an integrating sphere. ^cToo weak photoluminescence to measure.

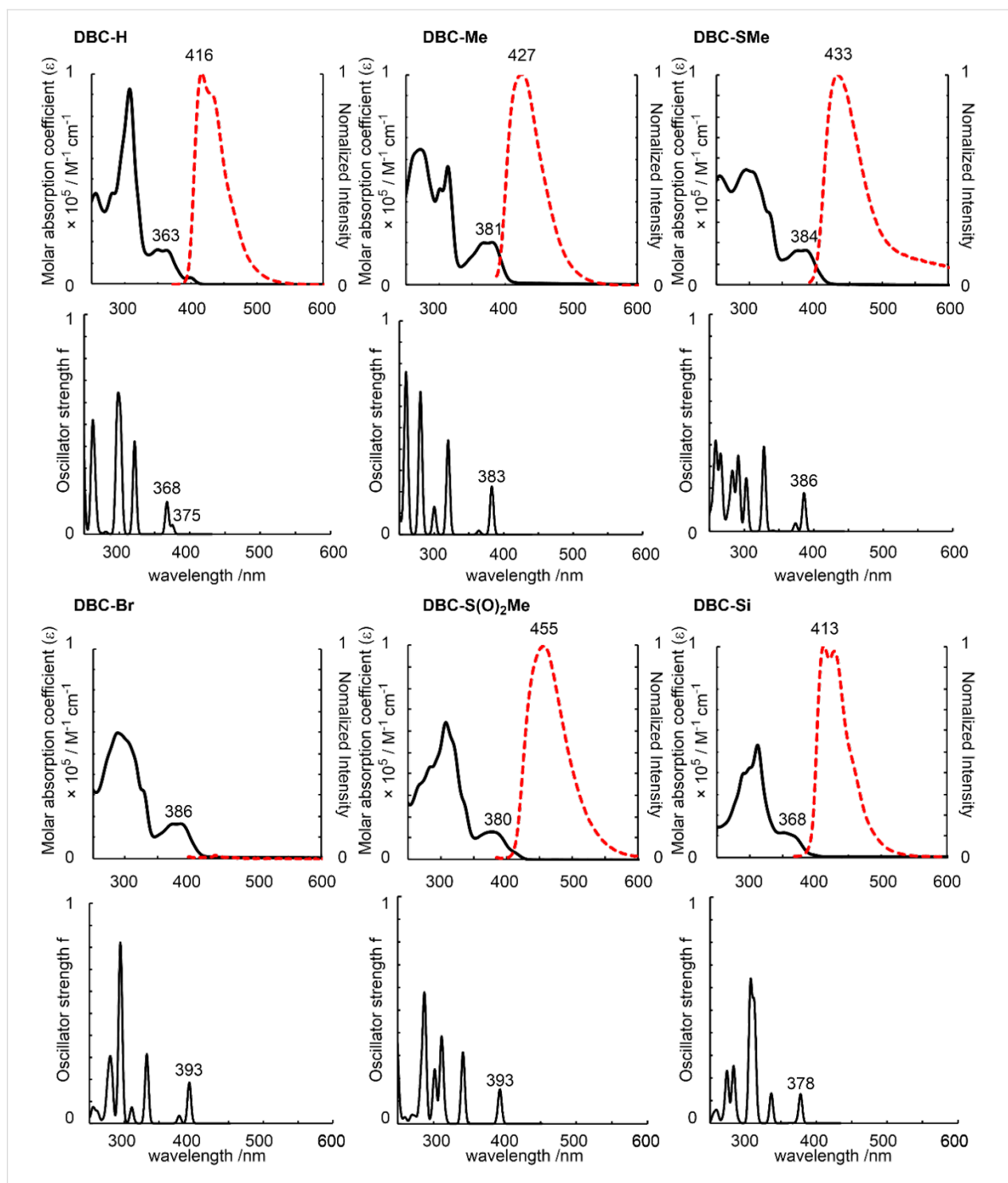


Figure 4: Absorption (solid line) and photoluminescence (dotted red line) spectra (upper graphs) in CH_2Cl_2 and simulations of absorption based on TD-DFT calculations [lower graphs, TD-B3LYP-D3/6-31G(d,p)//B3LYP/6-31G(d,p)] for DBC derivatives.

Z position resulted in a higher oxidation potential than that for **DBC-H**, even for compounds that contained electron-donating groups, such as **DBC-Me** and **DBC-SMe**. DFT calculations clearly indicate that this is due to the ineffective conjugation of the MeO group which is oriented perpendicular to the aromatic

ring because of the steric repulsion of substituents on both sides. More specifically, the inductive effect of the MeO group is dominant rather than the mesomeric effect when the substituent is present at the Z position. Concerning the torsion of the naphthalene moiety, the twisting caused a slight increase in the

HOMO and a slight lowering of the LUMO. The twisting effect is much smaller than the conjugation effect of the MeO group. Absorption spectra of all the substituted DBC derivatives also showed a red-shift as compared to that for **DBC-H**. Concerning photoluminescence, a strong photoluminescence was observed for **DBC-H** and **DBC-Si**. The findings reported in this study will be useful for the molecular design of such materials, and could lead to electronic material applications in the future.

Supporting Information

Supporting Information File 1

Figures S1–S3, Tables S1–S6, general, experimental procedure, and cartesian coordinates of optimized structures obtained based on the theoretical calculation.

[<https://www.beilstein-journals.org/bjoc/content/supplementary/1860-5397-18-96-S1.pdf>]

Acknowledgements

The computation was performed using Research Center for Computational Science, Okazaki, Japan (Project: 21-IMS-C190, 22-IMS-C174). We thank Prof. Shinobu Aoyagi at Graduate School of Science, Nagoya City University for the use of a voltammetry analyser.

Funding

Tetsuo Iwasawa is grateful to JSPS Grant-in-Aid for Scientific Research (C) (22K05086) and 2022 the Joint Research Center for Science and Technology of Ryukoku University.

ORCID® iDs

Toru Amaya - <https://orcid.org/0000-0002-7716-0630>

Tetsuo Iwasawa - <https://orcid.org/0000-0002-1068-2733>

References

- Clar, E. *Polycyclic hydrocarbons*; Academic Press: London, UK, 1964; Vol. I,II.
- Harvey, R. G. *Polycyclic Aromatic Hydrocarbons*; Wiley-VCH: New York, NY, USA, 1997.
- Fetzer, J. C. *Large Polycyclic Aromatic Hydrocarbons*, 1st ed.; *Chemistry and Analysis*, Vol. 158; John Wiley & Sons: Hoboken, NJ, USA, 2000.
- Anthony, J. E. *Chem. Rev.* **2006**, *106*, 5028–5048. doi:10.1021/cr050966z
- Sergeyev, S.; Pisula, W.; Geerts, Y. H. *Chem. Soc. Rev.* **2007**, *36*, 1902–1929. doi:10.1039/b417320c
- Anthony, J. E. *Angew. Chem., Int. Ed.* **2008**, *47*, 452–483. doi:10.1002/anie.200604045
- Pisula, W.; Feng, X.; Müllen, K. *Chem. Mater.* **2011**, *23*, 554–567. doi:10.1021/cm102252w
- Wang, C.; Dong, H.; Hu, W.; Liu, Y.; Zhu, D. *Chem. Rev.* **2012**, *112*, 2208–2267. doi:10.1021/cr100380z
- Sun, Z.; Ye, Q.; Chi, C.; Wu, J. *Chem. Soc. Rev.* **2012**, *41*, 7857–7889. doi:10.1039/c2cs35211g
- Zhang, D.; Duan, L. *J. Phys. Chem. Lett.* **2019**, *10*, 2528–2537. doi:10.1021/acs.jpcllett.9b00526
- Tian, D.; Chen, Y. *Adv. Opt. Mater.* **2021**, *9*, 2002264. doi:10.1002/adom.202002264
- Li, Q.; Zhang, Y.; Xie, Z.; Zhen, Y.; Hu, W.; Dong, H. *J. Mater. Chem. C* **2022**, *10*, 2411–2430. doi:10.1039/d1tc04866j
- Yao, T.; Yu, H.; Vermeij, R. J.; Bodwell, G. J. *Pure Appl. Chem.* **2008**, *80*, 533–546. doi:10.1351/pac200880030533
- Petrukhina, M. A.; Scott, L. T., Eds. *Fragments of Fullerenes and Carbon Nanotubes*; John Wiley & Sons: Hoboken, NJ, USA, 2011. doi:10.1002/9781118011263
- Wu, Y.-T.; Siegel, J. S. *Chem. Rev.* **2006**, *106*, 4843–4867. doi:10.1021/cr050554q
- Tsefrikas, V. M.; Scott, L. T. *Chem. Rev.* **2006**, *106*, 4868–4884. doi:10.1021/cr050553y
- Gingras, M. *Chem. Soc. Rev.* **2013**, *42*, 968–1006. doi:10.1039/c2cs35154d
- Amaya, T.; Hirao, T. *Chem. Rec.* **2015**, *15*, 310–321. doi:10.1002/tcr.201402078
- Ball, M.; Zhong, Y.; Wu, Y.; Schenck, C.; Ng, F.; Steigerwald, M.; Xiao, S.; Nuckolls, C. *Acc. Chem. Res.* **2015**, *48*, 267–276. doi:10.1021/ar500355d
- Segawa, Y.; Ito, H.; Itami, K. *Nat. Rev. Mater.* **2016**, *1*, 15002. doi:10.1038/natrevmats.2015.2
- Chen, C.-F.; Shen, Y. *Helicene Chemistry*; Springer: Berlin, Heidelberg, 2017. doi:10.1007/978-3-662-53168-6
- Saito, M.; Shinokubo, H.; Sakurai, H. *Mater. Chem. Front.* **2018**, *2*, 635–661. doi:10.1039/c7qm00593h
- Pascal, R. A., Jr. *Chem. Rev.* **2006**, *106*, 4809–4819. doi:10.1021/cr050550l
- Rickhaus, M.; Mayor, M.; Juriček, M. *Chem. Soc. Rev.* **2016**, *45*, 1542–1556. doi:10.1039/c5cs00620a
- Ma, S.; Gu, J.; Lin, C.; Luo, Z.; Zhu, Y.; Wang, J. *J. Am. Chem. Soc.* **2020**, *142*, 16887–16893. doi:10.1021/jacs.0c08555 and references cited therein.
- Herbstein, F. H. *Acta Crystallogr., Sect. B: Struct. Crystallogr. Cryst. Chem.* **1979**, *35*, 1661–1670. doi:10.1107/s0567740879007354
- Tokito, S.; Noda, K.; Fujikawa, H.; Taga, Y.; Kimura, M.; Shimada, K.; Sawaki, Y. *Appl. Phys. Lett.* **2000**, *77*, 160–162. doi:10.1063/1.126910
- Yamaguchi, S.; Swager, T. M. *J. Am. Chem. Soc.* **2001**, *123*, 12087–12088. doi:10.1021/ja016692o
- Kumar, S.; Varshney, S. K. *Mol. Cryst. Liq. Cryst. Sci. Technol., Sect. A* **2002**, *378*, 59–64. doi:10.1080/713738586
- Li, C.-W.; Wang, C.-I.; Liao, H.-Y.; Chaudhuri, R.; Liu, R.-S. *J. Org. Chem.* **2007**, *72*, 9203–9207. doi:10.1021/jo701504m
- Chaudhuri, R.; Hsu, M.-Y.; Li, C.-W.; Wang, C.-I.; Chen, C.-J.; Lai, C. K.; Chen, L.-Y.; Liu, S.-H.; Wu, C.-C.; Liu, R.-S. *Org. Lett.* **2008**, *10*, 3053–3056. doi:10.1021/ol801029x
- Shimizu, M.; Nagao, I.; Tomioka, Y.; Hiyama, T. *Angew. Chem., Int. Ed.* **2008**, *47*, 8096–8099. doi:10.1002/anie.200803213
- Navale, T. S.; Zhai, L.; Lindeman, S. V.; Rathore, R. *Chem. Commun.* **2009**, 2857–2859. doi:10.1039/b903133b
- Mori, T.; Fujita, K.; Kimura, M. *J. Photopolym. Sci. Technol.* **2010**, *23*, 317–322. doi:10.2494/photopolymer.23.317

35. Tsuji, H.; Ueda, Y.; Ilies, L.; Nakamura, E. *J. Am. Chem. Soc.* **2010**, *132*, 11854–11855. doi:10.1021/ja1059119
36. Navale, T. S.; Thakur, K.; Rathore, R. *Org. Lett.* **2011**, *13*, 1634–1637. doi:10.1021/ol200069c
37. Mochida, K.; Kawasumi, K.; Segawa, Y.; Itami, K. *J. Am. Chem. Soc.* **2011**, *133*, 10716–10719. doi:10.1021/ja202975w
38. Ueda, Y.; Tsuji, H.; Tanaka, H.; Nakamura, E. *Chem. – Asian J.* **2014**, *9*, 1623–1628. doi:10.1002/asia.201402102
39. Hashimoto, S.; Ikuta, T.; Shiren, K.; Nakatsuka, S.; Ni, J.; Nakamura, M.; Hatakeyama, T. *Chem. Mater.* **2014**, *26*, 6265–6271. doi:10.1021/cm503102d
40. Suzuki, N.; Fujita, T.; Ichikawa, J. *Org. Lett.* **2015**, *17*, 4984–4987. doi:10.1021/acs.orglett.5b02426
41. Liu, X.-Y.; Tang, X.; Zhao, Y.; Zhao, D.; Fan, J.; Liao, L.-S. *Dyes Pigm.* **2017**, *146*, 234–239. doi:10.1016/j.dyepig.2017.06.036
42. Song, S.; Huang, G.; Kojima, T.; Nakae, T.; Uno, H.; Sakaguchi, H. *Chem. Lett.* **2017**, *46*, 1525–1527. doi:10.1246/cl.170614
43. Ivanov, M. V.; Talipov, M. R.; Navale, T. S.; Rathore, R. *J. Phys. Chem. C* **2018**, *122*, 2539–2545. doi:10.1021/acs.jpcc.7b11232
44. Wang, S.; Yang, P.; Chang, K.; Lv, W.; Mi, B.; Song, J.; Zhao, X.; Gao, Z. *Org. Electron.* **2019**, *74*, 269–275. doi:10.1016/j.orgel.2019.07.022
45. Kogashi, K.; Matsuno, T.; Sato, S.; Isobe, H. *Angew. Chem., Int. Ed.* **2019**, *58*, 7385–7389. doi:10.1002/anie.201902893
46. Suzuki, Y.; Tohnai, N.; Saeki, A.; Hisaki, I. *Chem. Commun.* **2020**, *56*, 13369–13372. doi:10.1039/d0cc06081j
47. Yoshida, N.; Kamiguchi, S.; Sakao, K.; Akasaka, R.; Fujii, Y.; Maruyama, T.; Iwasawa, T. *Tetrahedron Lett.* **2020**, *61*, 152033. doi:10.1016/j.tetlet.2020.152033
48. Yoshida, N.; Kamiguchi, S.; Fujii, Y.; Sakao, K.; Maruyama, T.; Tokai, S.; Matsumoto, Y.; Taguchi, Y.; Akasaka, R.; Iwasawa, T. *Tetrahedron Lett.* **2020**, *61*, 152406. doi:10.1016/j.tetlet.2020.152406
49. Fujii, Y.; Maruyama, T.; Akasaka, R.; Sakao, K.; Tokai, S.; Taguchi, Y.; Matsumoto, Y.; Kamiguchi, S.; Yoshida, N.; Iwasawa, T. *Tetrahedron Lett.* **2021**, *65*, 152758. doi:10.1016/j.tetlet.2020.152758
50. Fujii, Y.; Taguchi, Y.; Tokai, S.; Matsumoto, Y.; Yoshida, N.; Iwasawa, T. *Tetrahedron* **2021**, *95*, 132353. doi:10.1016/j.tet.2021.132353
51. Yoshida, N.; Akasaka, R.; Awakura, Y.; Amaya, T.; Iwasawa, T. *Eur. J. Org. Chem.* **2021**, 5343–5347. doi:10.1002/ejoc.202100869
52. Kamiguchi, S.; Akasaka, R.; Yoshida, N.; Imai, T.; Yamaoka, Y.; Amaya, T.; Iwasawa, T. *Tetrahedron Lett.* **2022**, *92*, 153664. doi:10.1016/j.tetlet.2022.153664
53. The voltammograms including the low potential region for **DBC-SMe** and **DBC-S(O)₂Me** are shown in Figure S1 (Supporting Information File 1). Other DBC derivatives did not show any peaks in the low potential region.
54. The HOMO and LUMO energy levels for **DBC-H**, **DBC-Me**, **DBC-SMe**, **DBC-Br**, **DBC-S(O)₂Me**, and **DBC-Si** based on DFT calculations were reported in a previous paper together with the optimized structure and HOMO and LUMO orbital drawings (Supporting Information File 1 in reference [52]).
55. Cardona, C. M.; Li, W.; Kaifer, A. E.; Stockdale, D.; Bazan, G. C. *Adv. Mater. (Weinheim, Ger.)* **2011**, *23*, 2367–2371. doi:10.1002/adma.201004554
56. DFT calculations for **DBC-H(56°)-1** and **DBC-H(56°)-2** were performed in this study.
57. Bedi, A.; Gidron, O. *Acc. Chem. Res.* **2019**, *52*, 2482–2490. doi:10.1021/acs.accounts.9b00271
58. TD-DFT calculations for **DBC-H**, **DBC-Me**, **DBC-SMe**, **DBC-Br**, **DBC-S(O)₂Me**, and **DBC-Si** were performed in this study. Tables S1–S6 in Supporting Information File 1 show the wavelengths and oscillator strengths for the DBC derivatives.

License and Terms

This is an open access article licensed under the terms of the Beilstein-Institut Open Access License Agreement (<https://www.beilstein-journals.org/bjoc/terms>), which is identical to the Creative Commons Attribution 4.0 International License (<https://creativecommons.org/licenses/by/4.0>). The reuse of material under this license requires that the author(s), source and license are credited. Third-party material in this article could be subject to other licenses (typically indicated in the credit line), and in this case, users are required to obtain permission from the license holder to reuse the material.

The definitive version of this article is the electronic one which can be found at:

<https://doi.org/10.3762/bjoc.18.96>